12. Pretorius PH, Van Aswegen A, Herbst CP, Lötter MG. The effects of different correction techniques on absolute volume determination with SPECT using a threshold edge detection method. *Med Phys* 1991;18:390–393.
13. Nelson AD, Muswick GJ, Muzic RF, Deschamps X. A robust edge detection method for gated radionuclide ventriculograms. *J Nucl Med* 1996;37:685–689.
14. Arcilla RA, Tsai P, Thilenius O, Ranniger K. Angiocardiographic method for volume estimation of right and left ventricle. *Chest* 1971;60:446–454.
15. Gentzler RD, Briselli MF, Gault JH. Angiographic estimation of right ventricular volume in man. *Circulation* 1974;50:324–330.
16. Starling MR, Crawford MH, Sorensen SG, O'Rouke RA. A new two-dimensional echocardiographic technique for evaluating right ventricular size and performance in patients with obstructive lung disease. *Circulation* 1982;66:612–620.
17. Bommer W, Weinert L, Neumann A, Neef J, Mason DT, DeMaria A. Determination of right atrial and right ventricular size by two-dimensional echocardiography. *Circulation* 1979;60:91–100.
18. Boxt LM, Katz J, Kolb T, Barst RJ. Direct quantitation of right and left ventricular volumes using magnetic resonance imaging in patients with pulmonary hypertension. *J Am Coll Cardiol* 1992;19:1508–1515.
19. Benjelloun H, Cranney GB, Kirk KA, Blackwell GG, Lotan CS, Pohost GM. Interstudy reproducibility of biplane cine nuclear magnetic resonance measurements of left ventricular function. *Am J Cardiol* 67:1413–1420.
20. Reiter SJ, Rumberger JA, Feiring AJ, Stanford W, Marcus ML. Precision of measurements of right and left ventricular volume by cine computed tomography. *Circulation* 1986;74:890–900.
21. Hajduczok ZD, Weiss RM, Stanford W, Marcus ML. Determination of right ventricular mass in human and dogs with ultrafast computed tomography. *Circulation* 1990;82:202–212.
22. Terry JA. A receiver operating analysis of parallel, fan beam and cone beam collimator designs for cardiac single photon emission computed tomography imaging [PhD dissertation]. Chapel Hill, NC: University of North Carolina, 1992.
23. Tsui BMW, Zhoa XD, Gregoriou GK, et al. Quantitative cardiac SPECT reconstruction with reduced image degradation due to patient anatomy. *IEEE Trans Nucl Sci* 1994;41:2838–2844.
24. Xia W, Tsui BMW, King MA, Villegas BJ. Cardiac motion simulation and study of its influence on the polar map of the left ventricular wall [Abstract]. *J Nucl Med* 1995;36:59P.
25. Pretorius PH, Xia W, King MA, Tsui BMW, Pan T-S, Villegas BJ. Determination of left and right ventricular volume and ejection fraction using a mathematical cardiac torso phantom for gated blood pool SPECT [Abstract]. *J Nucl Med* 1996;37:97P.
26. Snyder WS, Cook MJ, Nasset ES, Karhausen LR, Howells GP, Tipton IH. Report of the task group on the reference man. ICRP Series 23, 1974.
27. Coffey JL. A revised mathematical model of the heart for use in radiation absorbed dose calculation [MS dissertation]. Knoxville, TN: University of Tennessee, 1978.
28. Guyton AC. *Textbook of medical physiology*, 7th ed. Philadelphia: WB Saunders; 1986:150–164.
29. Weyman AE. *Principles and practices of echocardiography*, 2nd ed. Philadelphia: Waverly; 1994:1290–1294.
30. Yang SS, Bentivoglio LG. *From cardiac catheterization data to hemodynamic parameters*, 3rd ed. Philadelphia: FA Davis; 1988:102–105.
31. Bacharach SL, Green MV, Borer JS, Hyde JE, Farkas SP, Johnston GS. Left-ventricle peak ejection rate, filling rate and ejection fraction: frame rate requirements at rest and exercise. *J Nucl Med* 1979;20:189–193.
32. Van Aswegen A, Alderson PO, Nickoloff EL, Housholder DF, Wagner HN Jr. Temporal resolution requirements for left ventricular time–activity curves. *Radiology* 1980;135:165–170.
33. Pan T-S, Luo D-S, King MA. Design of an efficient three-dimensional projector and backprojector pair for SPECT. In: *Proceedings of fully three-dimensional image reconstruction in radiology and nuclear medicine*. Aix-les-Bains, Savorie, France 1995:181–185.
34. King MA, Hademenos GJ, Glick SJ. A dual-photopeak window method for scatter correction. *J Nucl Med* 1992;33:605–612.
35. Pretorius PH, Van Rensburg AJ, Van Aswegen A, Lötter MG, Serfontein DE, Herbst CP. The channel ratio method of scatter correction for radionuclide image quantitation. *J Nucl Med* 1993;34:330–335.
36. Jaszczak RJ, Greer KL, Floyd CE Jr, Harris CC, Coleman RE. Improved SPECT quantitation using compensation for scattered photons. *J Nucl Med* 1984;25:893–900.
37. Axelsson B, Msaki P, Israelsson A. Subtraction of compton-scattered photons in single-photon emission computerized tomography. *J Nucl Med* 1984;25:490–494.
38. Ichihara T, Ogawa K, Motomura N, Kubo A, Hashimoto S. Compton scatter compensation using the triple-energy window method for single- and dual-isotope SPECT. *J Nucl Med* 1993;34:2216–2221.
39. Chang LT. A method for attenuation correction in radionuclide computed tomography. *IEEE Trans Nucl Sci* 1978;25:638–643.
40. Pollard JH. *A handbook of numerical and statistical techniques*. Cambridge, UK: Cambridge University Press; 1979:161–163.

Myocardial Perfusion Imaging with a Combined X-Ray CT and SPECT System

Kathrin Kalki, Stephen C. Blankespoor, J. Keenan Brown, Bruce H. Hasegawa, Michael W. Dae, Michael Chin and Carol Stillson

UCSF Physics Research Laboratory, Department of Radiology, Bioengineering Graduate Group and Cardiovascular Research Institute, University of California San Francisco, San Francisco, California

We evaluated a novel combined x-ray CT and SPECT medical imaging system for quantitative in vivo measurements of ^{99m}Tc-sestamibi uptake in an animal model of myocardial perfusion. **Methods:** Correlated emission-transmission myocardial images were obtained from 7- to 10-kg pigs. The x-ray CT image was used to generate an object-specific attenuation map that was incorporated into an iterative ML-EM algorithm for reconstruction and attenuation correction of the coregistered SPECT images. The pixel intensities in the SPECT images were calibrated in units of radionuclide concentrations (MBq/g), then compared against in vitro ^{99m}Tc activity concentration measured from the excised myocardium. In addition, the coregistered x-ray CT image was used to determine anatomical boundaries for quantitation of myocardial regions with low perfusion. **Results:** The accuracy of the quantitative measurement of in vivo activity concentration in the porcine myocardium was improved by object-specific attenuation correction. However, an additional correction for partial volume errors was required to retrieve the true activity concentration from the reconstructed SPECT images. **Conclusion:** Accurate absolute SPECT quantitation required object-specific correction for attenuation and partial volume effects. Additional anatomical information from the x-ray CT image was helpful in defining regions of interest for quantitation of the SPECT images.

Key Words: SPECT; quantification; myocardial perfusion; image coregistration

J Nucl Med 1997; 38:1535–1540

Absolute quantitation of radionuclide uptake from SPECT is compromised by photon attenuation, scattered radiation and partial volume errors (*1,2*). Therefore, several investigators have incorporated transmission measurements into reconstruction of the radionuclide image for compensation of photon attenuation. SPECT images also have been coregistered with images from x-ray CT or MRI (*3,4*) to improve anatomical definition, localization and quantitative accuracy of functional information obtained with SPECT.

We are developing a new imaging device, christened the emission-transmission CT (ETCT) system, which uses a common detector and imaging geometry to obtain a co-registered functional data from SPECT and anatomical data from x-ray CT. For quantitative measurements, the transmission CT image can be used to generate an object-specific attenuation map for attenuation compensation of the SPECT data. In this study we

Received Nov. 10, 1995; revision accepted Sep. 11, 1996.

For correspondence or reprints contact: Bruce Hasegawa, PhD, UCSF Physics Research Laboratory, 389 Oyster Point Blvd., Suite 1, So., San Francisco, CA 94080.

demonstrate quantitation of radiolabeled tracers in a porcine model of myocardial perfusion by comparing in vivo radiotracer uptake measurements from the ETCT system with in vitro uptake measurements obtained from excised tissue samples.

MATERIALS AND METHODS

System Description and Data Acquisition

Detailed descriptions of the emission-transmission CT (ETCT) system and phantom studies have been published elsewhere (*5–7*) and will be reviewed briefly here. The ETCT system uses a 23-element high-purity germanium (HPGe) array with a 2-mm detector pitch (*8*) to acquire both x-ray transmission and radionuclide emission data in a third-generation fanbeam geometry. The detector array is translated along a 35° arc centered at the x-ray focus to acquire a full projection set of the object. The x-ray tube and detector are mounted on a gantry that rotates both around a stationary object to provide a 22-cm reconstruction diameter. The data acquisition system has counting rates ($>10^6$ cps/channel) and energy resolution (14% at 140 keV) that allow the x-ray and radionuclide photons to be recorded with a single-detector array, in either simultaneous or sequential scans. Because of the small detector size, the ETCT prototype system presently requires about 2.5 hr to acquire a single SPECT slice with 1110-2220 MBq (30-60 mCi) of ^{99m}Tc and 1 hr for a single-slice x-ray CT scan.

The x-ray tube is operated at 100 kVp with 1 mA tube current. Transmission data were generated with the x-ray tube (100 kVp, 1 mA) filtered with 0.5 mm of gadolinium and were recorded with a 65- to 110-keV energy window. The ^{99m}Tc radionuclide data were recorded with a 20% symmetric energy window. The spatial resolutions of the SPECT and x-ray CT modes in the ETCT system were determined from resolution phantoms to be about 6 mm FWHM (SPECT) and 1.8 mm FWHM (x-ray CT). Both emission and transmission data were acquired with 193 detector bins at 2° increments over a 360° rotation angle. Emission sinograms contained approximately 5×10^5 total counts, while transmission sinograms contained approximately 5×10^8 counts.

Animal Study Protocol

Animal studies were performed with the ETCT system to obtain absolute in vivo measurements of myocardial radiotracer uptake compared to in vitro activity measurements from the excised heart. The animal study protocol was approved by the institutional committee on animal research. Six pigs (8–10 kg) were anesthesized, mechanically respirated and had their ECG monitored continuously. Before the imaging study 1110-2220 MBq (30–60 mCi) ^{99m}Tc-sestamibi was injected intravenously. In two pigs, the regional myocardial blood flow was modified by a vasodilator (dipyridamole) and in two other animals by LAD occlusion. The occlusion was maintained for 6 min (2 min during and 4 min after ^{99m}Tc-sestamibi injection) to allow for blood clearance of the radiopharmaceutical.

The animal was placed in an acrylic specimen tube, and x-ray CT images were obtained in a commercial x-ray CT scanner to identify an appropriate plane for the single-slice imaging study in the ETCT system. The animal and specimen tube then were transfered to the ETCT system where an ungated SPECT scan and an x-ray CT scan were acquired sequentially over 4–5 hr. Immediately after the imaging experiment, the animal was euthanized, and the imaging plane was marked by thin needles inserted through the thorax and myocardium. The heart was removed, and a 1-cm slice was dissected corresponding to the imaging plane. For the control animals, and for those receiving dipyridamole, the right ventricle was separated from the excised slice, and the left ventricle was divided into four roughly equal-sized pieces using the junction of right ventricle and anterior wall as a reference point. For occlusion experiments, the occlusion was repeated at the end of the imaging study, and a blue dye was injected to mark perfused and unperfused areas before euthanizing the animal. The unperfused, occluded tissue was isolated, and the normally perfused myocardium was divided into equal-sized samples. For each tissue sample the myocardial wall thickness was determined with a vernier caliper neglecting any fat and other nonmyocardial tissue. The individual tissue samples were weighed and their activities were measured by placing them on the face of a scintillation camera with a vial containing a known activity of ^{99m}Tc as a calibration source.

Image Reconstruction

X-ray CT data were reconstructed with filtered backprojection using a Ram-Lak filter to generate a 256 × 256 image (1.1-mm pixel width). Transmission images also were reconstructed as 64 × 64 and 128 × 128 images, corresponding to the spatial resolution of the emission images, for use as attenuation maps. The x-ray CT transmission image was linearly scaled to generate an object-specific map of attenuation coefficients. The scaling factor was determined by dividing the tabulated value for water $\mu = 0.152$ cm^{-1} at 140 keV photon energy by the CT value obtained from an uniform water phantom. This scaling factor used to scale all regions (bone, soft tissue, lung) of the CT images.

SPECT images were reconstructed using 30 iterations of an iterative maximum likelihood-expectation maximization (ML-EM) algorithm (*9, 10*) with and without attenuation correction. Images were reconstructed as 128 × 128 or 64 × 64 images corresponding to pixel widths of 2.2 mm and 4.4 mm, respectively. No scatter correction was performed, but the emission data were corrected for physical decay. In the reconstructed emission images, pixel values were calibrated in absolute units (MBq/g) using tomographic data from a 20-cm diameter cylindrical phantom filled with a known uniform concentration of ^{99m}Tc and reconstructed with attenuation correction. Measurements on a thorax-like phantom containing various attenuating materials (air, water and Teflon™) verified that the activity concentration could be reconstructed to ± 8% of the true value.

Radionuclide Quantitation

ROIs were defined on the SPECT images to correspond to the excised tissue samples in the reconstructed SPECT images using a thresholding technique to segment the myocardium from background regions. When the segmentation procedure failed to separate the myocardium from background due to a perfusion defect, an outer boundary estimate for the myocardium was defined by outlining the heart contour in the correlated x-ray CT image. The mean pixel value in each ROI was calibrated in units MBq/g as described above. Therefore, for each ROI, the in vivo activity uptake, the in vitro activity uptake and the in vitro measured wall thickness were known.

A linear regression line was determined to compare in vivo and in vitro measurements, using the in vitro measurements as independent variables. Individual errors of 20% in the measured activity concentration resulting from errors due to reconstruction noise, pixel calibration and ROI selection were assumed for each in vivo value. We also estimated an in vivo value of 0.01 MBq/g from the background of the reconstructed SPECT images for a region with zero in vitro activity uptake.

Correction for Partial-Volume Effects

Recovery coefficients (*11*) for the true activity concentration were determined from a SPECT resolution phantom containing cylindrical hot lesions with diameters between 5 mm and 38 mm. The ratio of the mean pixel value in each lesion relative to that in the largest lesion (38 mm diameter) was then plotted as a function

of lesion diameter (Fig. 1). We deduced from this curve that for 7-mm objects, typical of the left ventricular wall, only half of the true activity is recovered and for 3-mm objects, typical of the right ventricular wall, only 35% is recovered. In this study, we used these results to define recovery coefficients to correct ROI-based activity measurements obtained from the SPECT images.

RESULTS

Attenuation Correction

The inherent coregistration obtained with the ETCT system is shown in an overlay (Fig. 2) of a high-resolution x-ray CT and the corresponding SPECT image generated without using any markers or postacquisition registration procedures. This demonstrates that the ETCT system aligns the CT-derived attenuation map with the SPECT imaging plane and allows the distribution of the radioactive tracer to be located accurately in the coregistered x-ray CT image.

The attenuation map is shown as a 256 × 256 matrix in Figure 3 with horizontal and vertical profiles. The values of the reconstructed attenuation coefficients correspond well to the tabulated values with the exception of bone. These results indicate that our calibration method, which is based on a linear scaling of the attenuation coefficient for water, is only approximate, especially for high Z material such as bone (*12*). However, we neglected the underestimated attenuation coefficient for bone since these regions contributed only a few isolated pixels to the attenuation map.

We also compared SPECT images reconstructed with the object-specific attenuation map against SPECT images reconstructed with homogeneous or no attenuation correction (Fig. 4). Global variations in SPECT pixel intensity were assessed by defining a 17 × 17 pixel around the mycoardium, in which the sum of all pixels was about 10% with homogeneous attenuation correction and 50% lower with no attenuation correction, compared with the image reconstruction with object-specific attenuation correction. To investigate whether the regional distribution of intensity throughout the myocardium is affected, the maximum pixel values in the 17 × 17 myocardial region were normalized to the maximum value within the same region defined for the attenuation-corrected image. Difference images were formed between the attenuation-corrected image and the normalized images reconstructed with homogeneous attenuation correction or with no correction. The pixel values in resulting difference images were as high as 10% relative to pixel values in the attenuation-corrected images, with the largest error occurring primarily in the pericardial areas and near the posterior wall. These results imply that the accuracy of quantitation of SPECT images depends on whether an object-specific or homogeneous attenuation correction is used for image reconstruction. Although these effects are rather subtle for data acquired from small animals used in this study, these results show that homogeneous or no attenuation correction causes the pixel intensity not just to scale differently compared to SPECT images reconstructed with object-specific attenuation, but also can cause a difference in regional intensity distribution.

Quantitation of SPECT Images

The in vivo values of ^{99m}Tc-sestamibi uptake in myocardial SPECT images reconstructed without attenuation correction are plotted in Figure 5 against corresponding in vitro activity uptake values obtained directly from the excised tissue samples. For a total number of n = 30 samples (i.e., five tissue samples per myocardial slice) we obtained a correlation coefficient of r = 0.77 between the two measurements. However, the in vivo

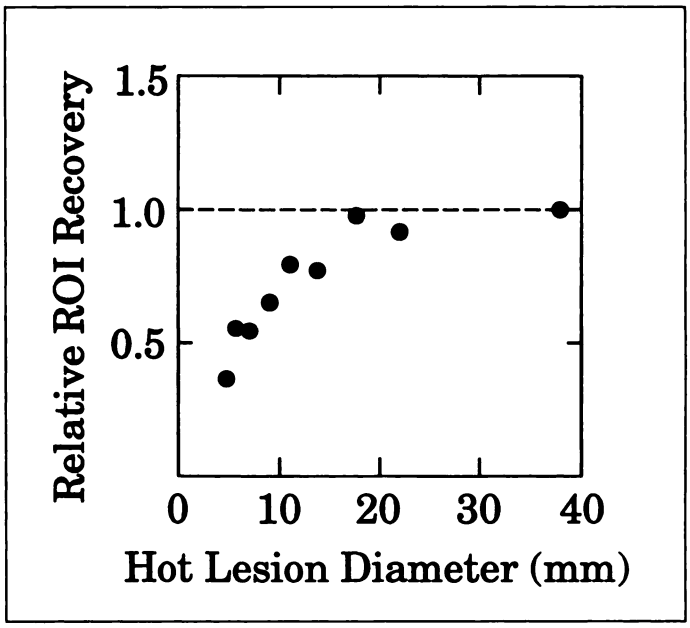

FIGURE 1. Measured activity concentration relative to the true activity concentration in each hot lesion as a function of lesion diameter. The 50% brightest pixels in each lesion were used to determine the mean pixel intensity.

uptake measurement is clearly too low compared to the true in vitro activity concentrations, as reflected in the slope of the regression line y = 0.17 (± 0.03) x + 0.01 (± 0.002) MBq, where y and x denote the in vivo and in vitro activity uptake, respectively, with their standard deviations given in parenthesis. If the SPECT reconstruction is performed with an object-specific attenuation map quantified using the same ROIs, the correlation coefficient does not change significantly (r = 0.84), but the in vivo values are higher (y = 0.42 (±0.02) x + 0.01 (±0.03)MBq) (Fig. 5B). Therefore, even with object-specific attenuation correction, only about 40% of the true activity was recovered from the reconstructed SPECT images.

Consequently, additional factors must be considered to improve accuracy in the in vivo activity uptake measurement. For example, partial volume errors occur in the radionuclide image since the mean myocardial wall thickness of the left ventricle (measured with calipers from the excised tissue samples) was only 7 ± 1.5 mm for all imaged heart slices, while the mean

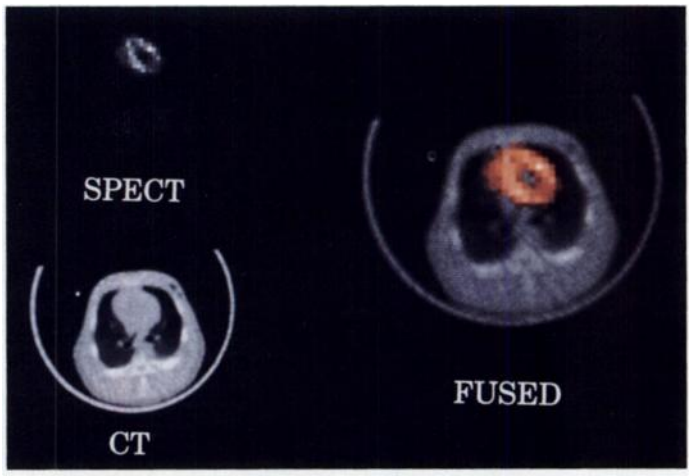

FIGURE 2. Overlay of x-ray CT (gray) and coregistered SPECT image (red) of a porcine thorax and myocardium. SPECT and CT images are separate (left). The combined SPECT/CT image (right).

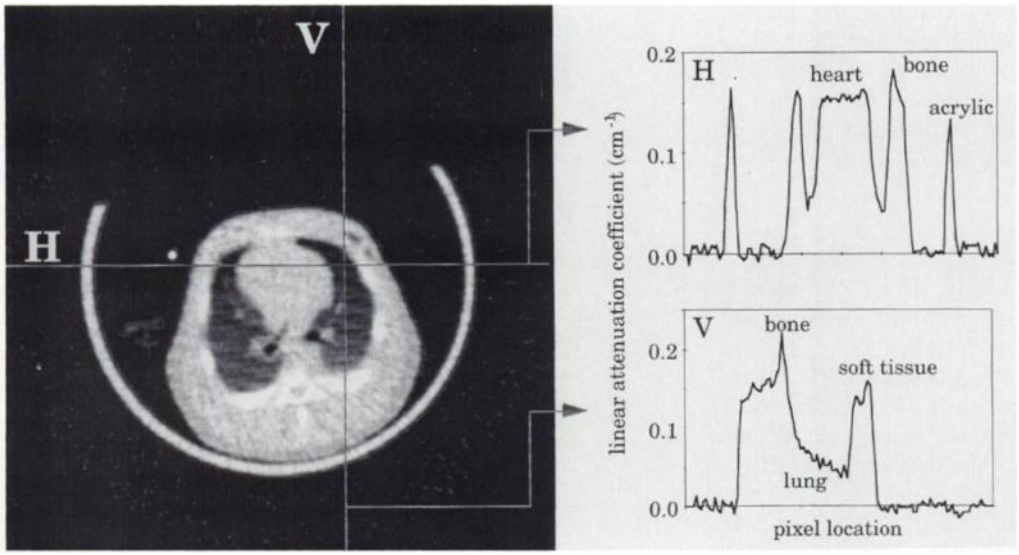

FIGURE 3. Linearly scaled attenuation map of the porcine thorax based on the attenuation coefficient of water at 140 keV. Two profiles through the map show the values of the linear attenuation coefficient for different materials.

thickness of the right ventricle was even smaller (3 ± 1 mm). Using these values, a recovery factor for the activity concentration was determined for the left ventricular wall (2.0) and the right ventricular wall (2.85) from the calibration curve (Fig. 1) as described in the Materials and Methods section. No attempt was made to correct ROIs individually with the corresponding wall thicknesses, since the wall thickness measured in vitro does not take into account wall motion that introduces an error of at least 1.5 mm between the in vivo and in vitro data. The corrections are, therefore, only approximate and potentially would be more accurate with an in vivo measurement of wall thickness. Nevertheless, Figure 5C shows that with correction for both attenuation and geometric system response, the quantitative agreement between in vivo and in vitro measurement of activity uptake is quite good ($y = 0.91\ (\pm 0.02)\ x + 0.01\ (\pm 0.002)$ MBq, $r = 0.81$). These results show that in the case of small animals imaged with the ETCT system, the accuracy of absolute SPECT quantitation is determined in roughly equal parts by proper attenuation correction and compensation for partial volume errors.

DISCUSSION

Numerous studies on phantoms, animals and humans demonstrate that correction for photon attenuation is crucial for obtaining an accurate measurement of radiotracer distribution using SPECT (*2,13,14*). Uniform attenuation maps can be used for correction of relatively homogeneous areas such as the head and abdomen, but for cardiac imaging, an object-specific attenuation correction is necessary to quantify regional myocardial perfusion accurately. In myocardial studies, the limited spatial resolution of the SPECT system also introduces artifactual inhomogeneities into the apparent radiotracer distribution (*15*). The relative effects of attenuation correction, spatial resolution and ROI selection on radionuclide quantitation have been studied here in a porcine model of myocardial perfusion using an imaging system that combines SPECT and x-ray CT.

In our SPECT study of small animals, attenuation correction proved to be straightforward since an object-specific attenuation map could be readily obtained from the coregistered x-ray CT image. Derivation of an object-specific attenuation map using linear scaling procedure of the polychromatic x-ray data

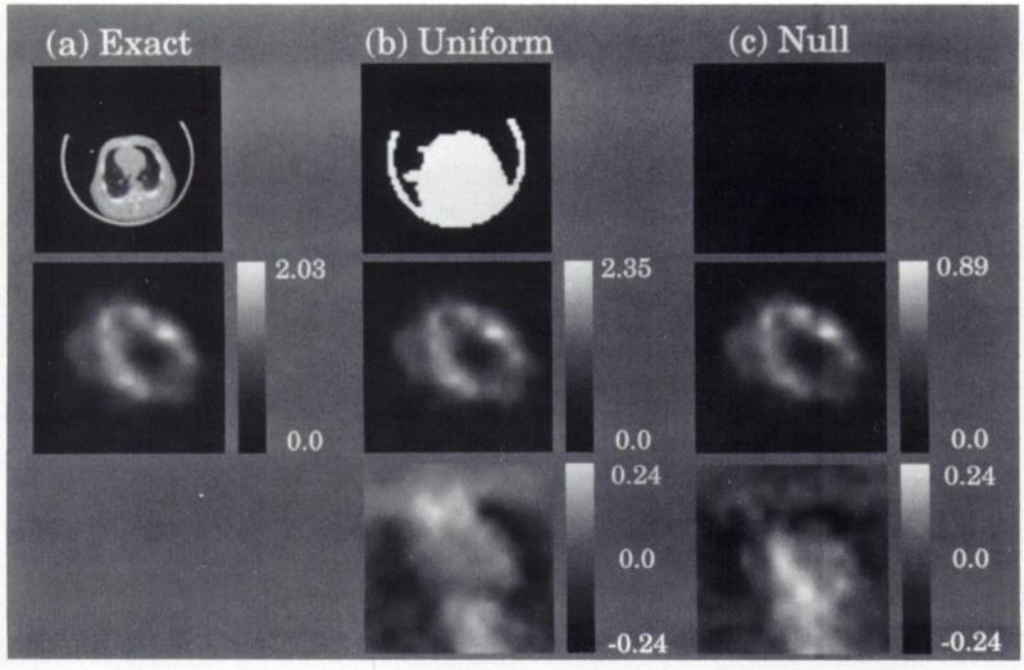

FIGURE 4. SPECT images of the porcine myocardium reconstructed with: (a) an object-specific attenuation map; (b) a homogeneous attenuation map using μ = 0.152 cm as attenuation coefficient for 140-keV photons; and (c) without attenuation correction. The attenuation maps are shown in the top row and myocardial ROIs of the reconstructed SPECT images in the middle row with gray scale bars indicating the pixel values in arbitrary units. Difference images between the SPECT ROI reconstructed with object-specific attenuation correction and SPECT images reconstructed without attenuation correction or homogeneous attenuation correction are shown in the bottom row with their pixel values.

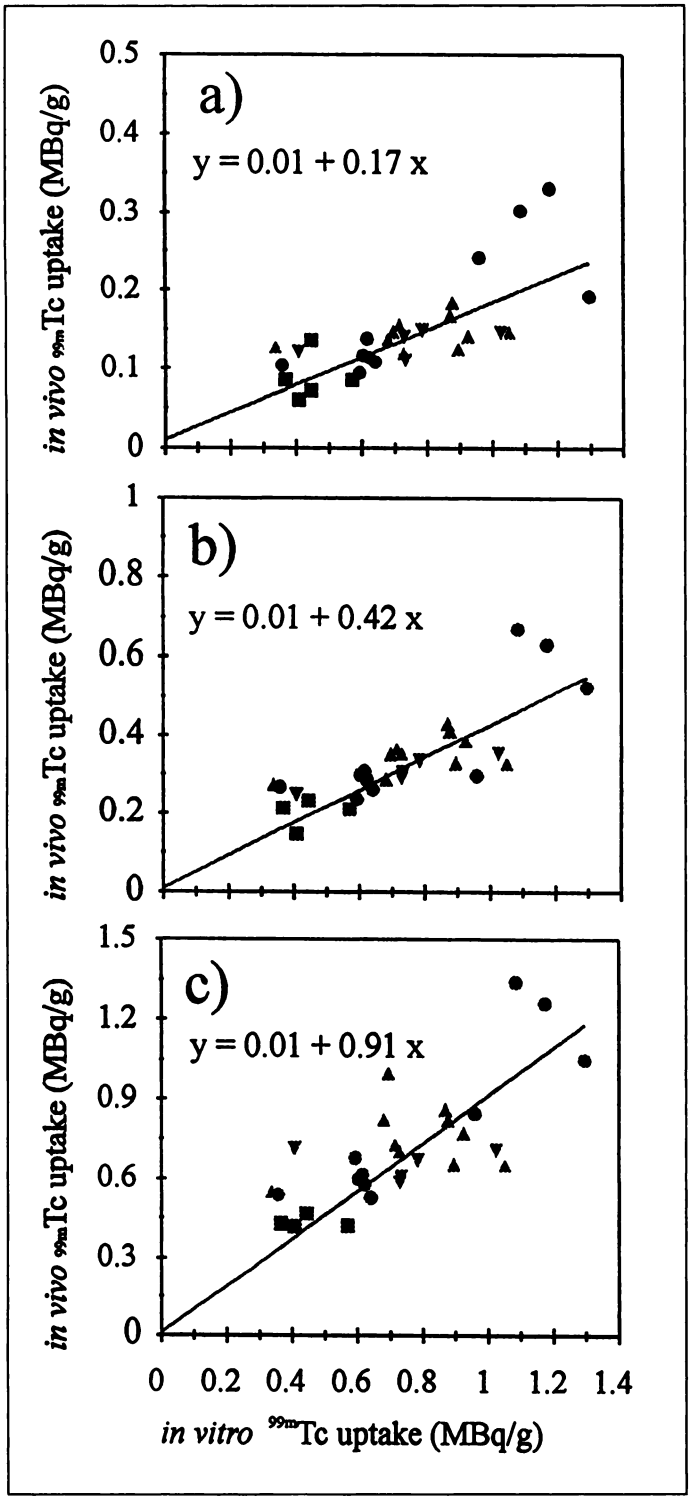

FIGURE 5. Comparison of ^{99m}Tc-sestamibi uptake measured from the reconstructed SPECT images in vivo and the corresponding excised tissue samples in vitro. SPECT images were reconstructed: (a) with no attenuation correction; (b) with object-specific attenuation correction; and (c) with both attenuation correction and correction for partial volume errors. Different symbols correspond to results from different animals.

proved to be sufficient for the relatively small animals imaged here. More accurate attenuation maps can be obtained with piece-wise calibration or with dual-energy techniques (*6,12*) and may be necessary for human studies, especially when higher levels of accuracy are needed.

However, our measurements show that object-specific attenuation correction only accounts for roughly 50% in the error in correlating in vivo and in vitro measurements of ^{99m}Tc concentration in the myocardium. The overall accuracy was markedly improved by correcting for partial volume errors. As pointed out before, we did not use any scatter correction schemes that might have further contributed to the inaccuracy of the quantitation, although a scatter contribution is contained in the pixel calibration factor obtained from the uniform water phantom and used for the animal SPECT images. However, if the mean scatter fraction (which is <30% for the uniformity phantom with our 20% energy windows) does not differ too much between the phantom and the animal study, then the difference in pixel value in the reconstructed image should be smaller than about 10% (*16*). Other factors, such as ROI selection and background subtraction, also are important in obtaining quantitatively accurate radionuclide measurements with SPECT. In addition, image blurring due to respiratory motion and myocardial wall motion decreases the precision of the uptake measurements (*15*) since ROI determination becomes less reproducible and less well defined.

Since SNR and spatial resolution of the transmission image are higher than for the corresponding emission image, the precision of the reconstructed SPECT image is expected to be influenced more by noise in the emission data than in the transmission data (*17, 18*). Moreover, partial volume errors and inaccuracies in ROI definition can be attacked in radionuclide images using correlated CT images since, in comparison to transmission images obtained with scanning line sources, those obtained with an x-ray source have improved spatial resolution (1.6 mm vs. 6 mm) and a significantly higher signal-to-noise ratio (by a factor of 100 or more). Our data do not show, in a statistically significant way, that x-ray CT supported ROI definition increases the precision of quantitation, but we are conducting further studies to substantiate our qualitative findings.

Practical Considerations

Results from the ETCT as reported in this manuscript are not intended to define specific methods of implementation, but do suggest that combining x-ray CT with SPECT in a direct way may improve quantitative assessment of internally distributed radiopharmaceuticals in comparison to conventional imaging techniques. At present, the long scan times and the small reconstruction circle obtained with our prototype system preclude clinical studies on humans with this device. However, these experimental results demonstrate that it is possible to record both emission and transmission datasets with a single detector, and upgrading our prototype system would provide proportionate improvements in scan times and detection sensitivity. Furthermore, emission-transmission systems have been proposed, which use commercially available detector technologies to combine x-ray CT and SPECT (*19*) or x-ray CT and PET (*20*) and may make emission-transmission systems possible and clinically practical.

CONCLUSION

We evaluated a novel combined x-ray CT and SPECT medical imaging system for quantitative in vivo measurements of ^{99m}Tc-sestamibi uptake in an animal model of myocardial perfusion. This was done using the x-ray CT image that was used to generate an object-specific attenuation map attenuation correction of the coregistered SPECT images. In correlated emission-transmission myocardial images from 7- to 10-kg pigs, the accuracy of the in vivo activity concentration measurement was improved by object-specific attenuation correction, but additional corrections for partial-volume errors were

required to retrieve the true myocardial activity concentration when compared against the in vitro ^{99m}Tc activity concentration measured from the excised myocardium.

AKNOWLEDGMENTS

This work was supported by National Cancer Institute grant 2 R01 CA50539 and by an American Heart Association Grant-in-Aid. We gratefully acknowledge financial support from the Whitaker Foundation. This work also was performed under the tenure of an Established Investigatorship from the American Heart Association for B.H. Hasegawa. We are grateful for an equipment loan from GE Medical Systems, Milwaukee, WI.

REFERENCES

1. Rosenthal MS, Cullom J, Hawkins W, Moore SC, Tsui BMW, Yester M. Quantitative SPECT imaging. A review and recommendations by the focus committee of the Society of Nuclear Medicine computer and instrumentation council. *J Nucl Med* 1995;36:1489–1513.
2. Tsui B, Frey E, Zhao X, Lalush D, Johnston R, McCartney H. The importance and implementation of accurate three-dimensional compensation methods for quantitative SPECT. *Phys Med Biol* 1994;39:509–530.
3. Kramer EL, Noz ME, Sanger JJ, Megibow AJ, Maguire GQ. CT-SPECT fusion to correlate radiolabeled monoclonal antibody uptake with abdominal CT findings. *Radiology* 1989;172:861–865.
4. Turkington TG, Jaszczak RJ, Pelizzari CA, Harrison CC, MacFall JR, Hoffman JM. Accuracy of registration of PET, SPECT and MR images of a brain phantom. *J Nucl Med* 1993;34:1587–1594.
5. Lang TF, Hasegawa BH, Liew SC, Brown JK, Blankespoor SC, Reilly SM. Description of a prototype emission-transmission CT imaging system. *J Nucl Med* 1992;33:1881–1887.
6. Hasegawa BH, Brown JK, Lang TF, Reilly SM, Liew SC, Gingold EL. Object-specific attenuation correction of SPECT with simultaneous x-ray CT. *IEEE Trans Nucl Sci* 1993;40:1242–1252.
7. Kalki K, Heanue JA, Blankespoor SC, Wu X, Brown JK, Cann CE. A combined SPECT and CT medical imaging system. *Proc SPIE* 1995;2432:367–375.
8. Hasegawa BH, Stebler B, Rutt BK, Martinez A, Gingold EL, Barker C. A prototype high-purity germanium detector system with fast photon-counting circuitry for medical imaging. *Med Phys* 1991;18:900–909.
9. Shepp LA, Vardi Y. Maximum likelihood reconstruction for emission tomography. *IEEE Trans Med Imag* 1982;MI-1:113–122.
10. Lange K, Carson R. EM reconstruction algorithms for emission and transmission tomography. *J Comput Assist Tomogr* 1984;8:306–316.
11. Kessler RM, Ellis JR, Eden M. Analysis of emission tomographic scan data: limitations imposed by resolution and background. *J Comput Assist Tomogr* 1984;8: 514–522.
12. LaCroix KJ, Tsui BMW, Hasegawa BH, Brown JK. Investigation of the use of x-ray CT images for attenuation correction in SPECT. *IEEE Trans Nucl Sci* 1994;41:2793–2799.
13. Tsui BMW, Gullberg GT, Edgerton ER, Ballard JG, Perry JR, McCartney WH. Correction of nonuniform attenuation in cardiac SPECT imaging. *J Nucl Med* 1989;30:497–507.
14. Li J, Jaszczak RJ, Greer KL, Gilland DR, DeLong DM, Coleman RE. Evaluation of SPECT quantification of radiopharmaceutical distribution in canine myocardium. *J Nucl Med* 1995;36:278–286.
15. Bartlett ML, Bacharach SL, Voipio-Pulkki LM, Dilsizian V. Artifactual inhomogeneities in myocaridal PET and SPECT scans in normal subjects. *J Nucl Med* 1995;36: 188–195.
16. Jaszczak RJ, Greer KL, Floyd CE. Improved SPECT quantification using compensation for scattered photons. *J Nucl Med* 1984;25:893–900.
17. Tung CH, Gullberg GT. A simulation of emission and transmission noise propagation in cardiac SPECT imaging with nonuniform attenuation correction. *Med Phys* 1993;21:1565–1576.
18. Liew SC, Hasegawa BH, Brown JK, Lang TF. Noise propagation in SPECT images reconstructed using an iterative maximum-likelihood algorithm. *Phys Med Biol* 1994;38:1713–1726.
19. Blankespoor SC, Hasegawa BH, Brown JK, Heanue JA, Gould RG, Cann CE. Development of an emission-transmission CT system combining x-ray CT and SPECT. *Conf Rec IEEE Nucl Sci Symp Med Imag Conf* 1994;4:1758–1761.
20. Beyer T, Kinahan PE, Townsend DW, Sashin D. The use of x-ray CT for attenuation correction of PET data. *Conf Rec IEEE Nucl Sci Symp Med Imag Conf* 1994;4: 1573–1577.

Effects of Cilazapril and Verapamil on Myocardial Iodine-125-Metaiodobenzylguanidine Accumulation in Cardiomyopathic BIO 53.58 Hamsters

Yasushi Wakabayashi, Chinori Kurata, Tadashi Mikami, Sakae Shouda, Kenichi Okayama and Kei Tawarahara

Department of Medicine III, Hamamatsu University School of Medicine, Hamamatsu, Japan

Sympathetic nervous system activation is important in the pathophysiology of congestive heart failure. However, little about how the treatment for heart failure may influence myocardial sympathetic nervous activity has been established. In this study, we evaluated effects of cilazapril (CLZ) and verapamil (VER) on myocardial sympathetic nervous activity in cardiomyopathic BIO 53.58 hamsters using [^{125}I]metaiodobenzylguanidine ([^{125}I]MIBG). **Methods:** We used BIO 53.58 hamsters aged 3, 6 and 10 mo and age-matched normal F1b hamsters. We divided BIO 53.58 hamsters into untreated, CLZ- and VER-treated groups. We measured myocardial [^{125}I]MIBG uptakes and norepinephrine concentrations and evaluated the extent of fibrosis and the distribution of [^{125}I]MIBG. **Results:** The myocardial [^{125}I]MIBG uptake was significantly lower in BIO 53.58 hamsters aged 6 and 10 mo than in age-matched F1b hamsters. Myocardial [^{125}I]MIBG uptake was significantly correlated to myocardial norepinephrine concentration in BIO 53.58 hamsters. Myocardial [^{125}I]MIBG uptake was significantly higher in both of the treated groups than in the untreated group. The extent of myocardial fibrosis was significantly lower in both of the treated groups than in the untreated group. The myocardial [^{125}I]MIBG uptake showed a significant inverse correlation with the extent of fibrosis. Myocardial [^{125}I]MIBG distribution was highly heterogeneous in the untreated BIO 53.58 hamsters, whereas it was homogeneous in the F1b hamsters aged 6 mo and the treated BIO 53.58 hamsters. **Conclusion:** In BIO 53.58 hamsters, myocardial [^{125}I]MIBG uptake decreased with the progression of cardiomyopathy, and the decreased uptake was improved by treatment with CLZ and VER. Thus, myocardial [^{125}I]MIBG uptake can reflect the effects of treatment on cardiomyopathy, as well as the progression of cardiomyopathy.

Key Words: iodine-125I-MIBG; cardiomyopathy; angiotensin-converting enzyme inhibitor; calcium antagonist; sympathetic nervous activity

J Nucl Med 1997; 38:1540–1545

Activation of the sympathetic nervous system is important in the pathophysiology of congestive heart failure (*1*). The concentration of norepinephrine (NE) in the coronary sinus or myocardium and myocardial NE spillover have been determined as indices of the myocardial sympathetic nervous activity (*2–4*). These methods, however, were invasive and unsuitable

Received Mar. 12, 1996; revision accepted Aug. 12, 1996.

For correspondence or reprints contact: Yasushi Wakabayashi, MD, Division of Cardiology, Iwata Municipal Hospital, 57-1 Kounodai, Iwata 438 Japan.